Satellite maneuver detection with optical survey observations

Alejandro Pastor
GMV, apastor@gmv.com
Guillermo Escribano
Universidad Carlos III de Madrid, guescrib@ing.uc3m.es

Diego Escobar
GMV, descobar@gmv.com

Abstract

The main source of potential new object detections during Resident Space Object (RSO) cataloging activities are maneuvers of operational satellites. Maneuver detection and estimation is thus deemed crucial for maintaining catalogs of RSOs as it helps to avoid sets of duplicated objects. For the continuous and reliable provision of Space Situational Awareness (SSA) and Space Traffic Management (STM) services, a challenging trade-off between detection time and characterization accuracy of maneuvers needs to be performed.

In this paper, two novel and operationally feasible methods are proposed to solve the correlation/association problem between pre-maneuver orbits and post-maneuver tracks (track-to-orbit) to detect and estimate single burn maneuvers and between pre-maneuver and post-maneuver orbits (orbit-to-orbit) to do so with multiple burns maneuvers. Such methods are based on an optimal control approach and aimed to be integrated on a Multiple Hypothesis Tracking (MHT) framework. Results are presented for optical survey scenarios with both simulated and real data, providing insightful conclusions on the capabilities and limitations of the proposed methods, emphasizing their suitability for operational and robust MHT frameworks.

1. INTRODUCTION

The increasing number of resident space objects (RSOs) and congestion of the orbital debris environment renders the space cataloging activities more challenging year after year. Currently, there are over 500 operational satellites only in Geostationary Earth Orbit (GEO) [1], most of which perform maneuvers every one or two weeks and for which Space Surveillance and Tracking (SST) systems mainly have optical observations. Such maneuvers represent the primary contribution to potential new detections, exceeding those related to satellite launches [2] and break-up events [3], so detecting them is crucial for maintaining catalogs of Resident Space Objects (RSOs). Capable maneuver detection and estimation methods are a must since otherwise these potential new detections would be promoted to actual new objects leading to sets of duplicated RSOs, thereby polluting the catalog and hampering the provision of Space Situational Awareness (SSA) and Space Traffic Management (STM) services.

The main issue for SST systems related to maneuvering RSOs is the challenging correlation of observations. In the case of survey sensors, correlation is usually performed by comparing real and simulated observations, generated from predicted orbits of already cataloged RSOs. Unless these predicted orbits take into account the maneuver plan followed by the operators (only possible for satellites providing the maneuver plan to the SST system), correlation analysis of the first track after a maneuver will fail for sufficiently high magnitude maneuvers and after enough time to impact the orbit. Even for tracking sensors this is a problem, since the RSOs might not be located where expected, therefore leading to an observability issue, which may result in a loss of the RSO or ambiguous correlation situations, where the originating RSO is not clear. In those cases, although the correlation would be achieved, maneuver estimation is still required to properly update the orbit of the RSO through orbit determination. The automatic detection of maneuvering RSOs can be framed within the general multi-target tracking-association problem, in which the tracked objects are allowed

Copyright © 2020 Advanced Maui Optical and Space Surveillance Technologies Conference (AMOS) – www.amostech.com

to maneuver. The approaches to the problem can be categorized in two broad categories: heuristic methods and stochastic filters.

The authors find it necessary to clarify some terms that are extensively used along this paper and whose meaning may vary from one author to another. On the one hand, we use the term *track* to refer to a set of observations taken by a single sensor usually over a short time period, originated from the same RSO and usually not enough to reliably estimate an orbit. Tracks from optical and radar surveillance sensors are usually referred to as uncorrelated optical observations (UCOs) and uncorrelated tracks (UCTs), respectively. We will refer to them as UCTs, regardless of the sensor type. On the other hand, a well-established estimation of the trajectory of an RSO in the catalog is called *orbit*. Accordingly, we refer to *track-to-track*, *track-to-orbit* and *orbit-to-orbit* as the association/correlation of tracks, tracks and orbits, and orbits, respectively.

Regarding track association for catalog maintenance, one can find the work of Stauch et al. [4] based on Joint Probabilistic Data Association (JPDA) [5] and Constrained Admissible Regions (CAR) [6], Pirovano et al. [7] still based on JPDA and CAR but with a different treatment for the uncertainty following Differential Algebra (DA) and that of Siminski et al. [8] and Furfaro et al. [9]. None of these methods is however capable of dealing with maneuvering objects, which may lead to object duplication if the maneuver exceeds the association uncertainty or likelihood.

To solve the maneuver detection and estimation problem, various methods have been proposed based on stochastic formulations. Holzinger & Scheeres [10] and Holzinger et al. [11] developed an alternative method to JPDA based on Distance Control Metrics as opposed to the usual Mahalanobis distance [12], which is aimed at determining the minimum required control effort to fit a given observation. Jia et al. [13] suggest an Interacting Multiple Models (IMM) approach based on two different process noise levels, expected for a non-maneuvering and maneuvering object respectively. Huang et al. [14] propose an interesting method for detecting maneuvers of space objects applicable only to Low Earth Orbit (LEO), where the velocity increment and maneuver epoch is estimated in the form of an optimal control problem, thereby significantly reducing the number of estimated variables. Nonetheless, the authors only consider orbit-to-orbit correlation as the maneuver epoch is guessed from the closest approach between the orbits of interest. The most efficient methods for GEO RSOs seem to be based on historical data (heuristics) since they typically perform repetitive Station Keeping (SK) maneuvers. In this regard, Siminski et al. [15] present an implementation based on actual maneuver data reported by the operator, whereas Lemmens and Krag [16] suggest utilizing Two Line Elements (TLEs) to characterize maneuvers. On the same topic, Shabarekh et al. [17] developed a machine learning approach aimed at determining Patterns of Life (PoL) in order to predict and characterize maneuvers.

Maneuver detection can be understood as an association/correlation problem and should be integrated within the cataloging chain used in this work, as depicted in Figure 2, which shows a view of the different processes involved. The very first UCT received after a maneuver will most likely not be reliably correlated against any RSO in the catalog due to the velocity change and its effects on the dynamics, so it enters into the track-to-track association algorithm, intended for the detection of new objects. Initially, this first post-maneuver UCT cannot be associated to any other track in this track-to-track process. As more post-maneuver UCTs are obtained, these can be associated. If nothing is done to detect the maneuvers, this would give rise to a new object at the end. In order to prevent this, depending on the complexity of the maneuver, there are two possibilities (branches 1 and 2 in Figure 2):

- **Single burn:** the new UCT is first associated with the corresponding orbit of the RSO via track-to-orbit correlation considering a single-burn maneuver (branch 1 in Figure 2). This allows to establish a first and preliminary link (association or hypothesis in the Multiple Hypothesis Tracking (MHT) framework) between an orbit and a single UCT, although the maneuver cannot be yet confirmed nor estimated reliably due to the scarce information available. The maneuver detection and estimation should be done in the observation space by means of a track-to-orbit correlation including maneuvers as described below, since the orbital estimation derived from the new UCT or the few associated UCTs is still not reliable enough to be directly used. As more UCTs after the maneuver arrive to the system, new associations of more tracks arise until there is enough information to promote, i.e. confirm, the hypothesized maneuver. The number of tracks for the association required to properly confirm and

Copyright © 2020 Advanced Maui Optical and Space Surveillance Technologies Conference (AMOS) – www.amostech.com

estimate a single burn maneuver (i.e., promote hypotheses) is expected to be around two or three, less than the four required for a full and nominal RSO initialization in the catalog [18, 19].

The track-to-orbit methodology proposed is able to detect maneuvers based on residuals between the estimated orbit before the maneuver and observations afterwards. Figure 1 shows the residuals of observations from four telescopes from the International Scientific Optical Network (ISON) network and a GEO satellite before and after a North-South maneuver (vertical dashed line). The more time after the maneuver is elapsed, the greater the divergence of the residuals becomes. This is an indication of the footprint of the maneuver on the residuals of the post-maneuver tracks if the pre-maneuver orbit is used in the residuals computation.

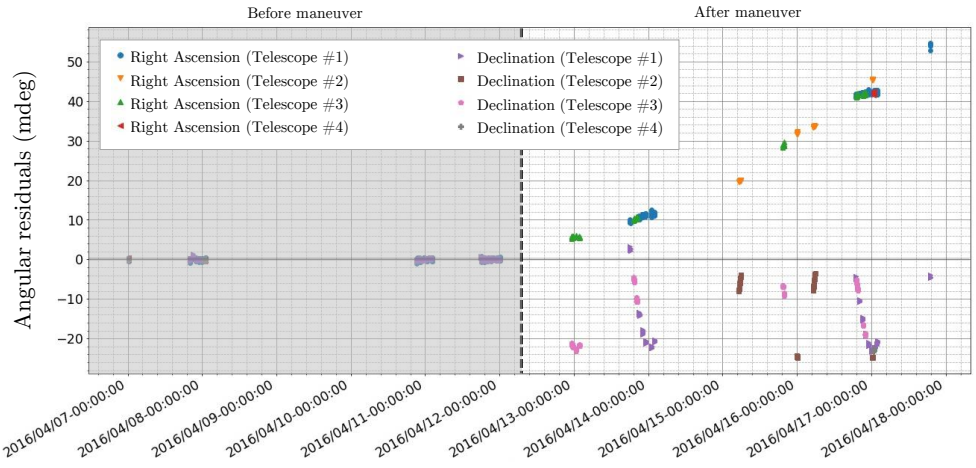

Figure 1: Residuals between the estimated orbit before the maneuver and measurements after the maneuver.

- **Multiple burns:** the information contained on a single track might not be enough to estimate the parameters characterizing a maneuver of multiple burns, since the track-to-orbit correlation algorithm including maneuvers and described above (branch 1 in Figure 2) would not be able to link the orbit with the post-maneuver UCTs. Therefore, it is required to associate a higher number of post-maneuver tracks to obtain a new and reliable orbit estimation without the use of prior information, i.e. perform a potential new RSO detection, by means of track-to-track correlation. The number of tracks required is higher than in the previous situation, since a full RSO initialization is performed, although initial estimates of the post-maneuver orbit can be derived allowing an early detection of the maneuver. Once accurate post-maneuver orbital information is available, the maneuver detection and estimation can be done in the orbit space by means of an orbit-to-orbit correlation considering maneuvers (branch 2 in Figure 2). This problem corresponds to the estimation of two maneuvers capable of linking two already well-established orbits. The case of low-thrust maneuvers is a challenge for this approach, but would still work as long as the low-thrust maneuver is finished, although the estimated impulsive maneuvers will not be very representative of the actual low-thrust maneuver performed.

Most of the aforecited methods must be tested and tuned for each specific application. The characteristics of the RSOs problem with scarcity of data and large time intervals between them makes the tuning demanding. In previous years, a series of works have tried to address the gaps of the classical approaches with methods developed ad-hoc for the SST problem [20, 21, 22, 23, 24]. In those works, RSO maneuvers are characterized a-priori, in order to incorporate more information to the problem, and make it more tractable. Nevertheless, most of them provide results for particular and isolated test cases, rather than representative enough scenarios, analogous to an operational SST system. Scalability concerns, as in the track association problem [18], is of a major importance, given the dimensions of the problem and the huge number of a-priori possible combinations to evaluate.

To address the above-mentioned gaps, we propose two maneuver detection and estimation methods to be used in our operational cataloging chain. They do not require any a-priori information of the maneuver and

Copyright © 2020 Advanced Maui Optical and Space Surveillance Technologies Conference (AMOS) – www.amostech.com

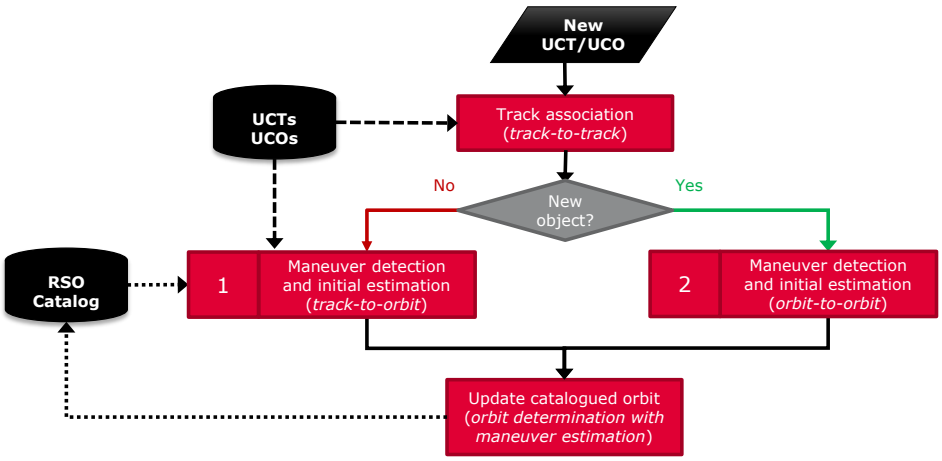

Figure 2: Maneuver detection and estimation role in the cataloging chain.

are able to provide an estimation to update the cataloged orbit of the involved RSO. To do so, associations of orbits and tracks, or hypotheses, are generated, evaluated, pruned and promoted in such a way that the involved cataloged orbit and sensing data belongs to a common maneuvered RSO. This allows to considerably reduce the maneuver detection time, since, as opposed to orbit-to-orbit association, a new object detection and initiation is not required. However, an alternative formulation is proposed to consider orbit-to-orbit correlation scenarios in which two established objects may be reduced to a single maneuvered one. Opposed to the single impulsive burn of the track-to-orbit correlation, this last orbit-to-orbit scenario assumes a double impulsive burn to allow for a transfer orbit capable of approximating maneuvers in a more robust manner.

The present paper is structured in four sections. Section 1 introduces the role of the maneuver detection and estimation on the cataloging activities, a state-of-the-art review and the framework of our proposal. Section 2 presents the two methods: track-to-orbit for single burn maneuver estimation and orbit-to-orbit for multiple burn maneuver estimation. Section 3 presents and discusses the results of two sets of cases for each method: 1) with synthetic observations and 2) with real observations. Finally, Section 4 gathers the conclusions of the paper and discuss the current status of the work.

2. METHODOLOGY

The two methods proposed for maneuver detection and estimation are presented in this section.

2.1 Single burn maneuver detection and estimation via track-to-orbit

On the one hand, we assume a pre-maneuver orbit (subscript A), i.e.: an orbit estimated before the maneuver, is available on the catalog. This means that an extended state vector:

$$\boldsymbol{y}_A(t) = [\boldsymbol{x}_A(t), \boldsymbol{p}_A]^T \in \mathbb{R}^{6+n_p} \tag{1}$$

is given, where $\boldsymbol{x}_A(t) = [\boldsymbol{r}_A(t), \boldsymbol{v}_A(t)]^T \in \mathbb{R}^6$ and $\boldsymbol{p}_A \in \mathbb{R}^{n_p}$ represent the state and dynamical parameters vectors, respectively, being $\boldsymbol{r}_A \in \mathbb{R}^3$ and $\boldsymbol{v}_A \in \mathbb{R}^3$ the corresponding position and velocity vectors.

On the other hand, a set of N optical observations, $\boldsymbol{z}(t_i) \in \mathbb{R}^2$ for $i = 1, \ldots, N$, has been received by the sensor network. Each observation contains a pair of right ascension and declination measurements referred to t_i, packed in tracks so that each track contains only observations from a common sensor over a short time period.

Copyright © 2020 Advanced Maui Optical and Space Surveillance Technologies Conference (AMOS) – www.amostech.com

Let $\boldsymbol{\Psi}(t, t_0)$ be the full transition matrix, allowing to propagate perturbations of the extended state vector from t_0 to t under the linear dynamics assumption, i.e.:

$$\boldsymbol{\Psi}(t, t_0) = \frac{\partial \boldsymbol{x}(t)}{\partial \boldsymbol{y}(t_0)} \in \mathbb{R}^6 \times \mathbb{R}^{6+n_p} \tag{2}$$

Note that $\boldsymbol{\Psi}(t, t_0)$ contains the so-called state transition, $\boldsymbol{\Phi}(t, t_0) = \partial \boldsymbol{x}(t)/\partial \boldsymbol{x}(t_0) \in \mathbb{R}^6 \times \mathbb{R}^6$, and sensitivity matrices, $\boldsymbol{S}(t, t_0) = \partial \boldsymbol{x}(t)/\partial \boldsymbol{p} \in \mathbb{R}^6 \times \mathbb{R}^{n_p}$. Subsets of these matrices will be referred to as $(\cdot)_{\alpha\beta}$, corresponding to $\partial \boldsymbol{\alpha}(t)/\partial \boldsymbol{\beta}(t_0)$.

At a certain epoch, t_M, an impulsive maneuver takes place causing a sudden change in the velocity, i.e.: $\boldsymbol{u} = \boldsymbol{v}_B(t_M) - \boldsymbol{v}_A(t_M)$, as shown in Figure 3. Since the position of the two orbits is intersecting at t_M, i.e.; $\boldsymbol{r}_A(t_M) = \boldsymbol{r}_B(t_M)$, the post-maneuver state (subscript B) can be obtained by considering the maneuver a perturbation at time t_i as follows:

$$\boldsymbol{x}_B(t) = \boldsymbol{x}_A(t) + \boldsymbol{\Psi}_{xv}(t, t_M)\,\boldsymbol{u} \tag{3}$$

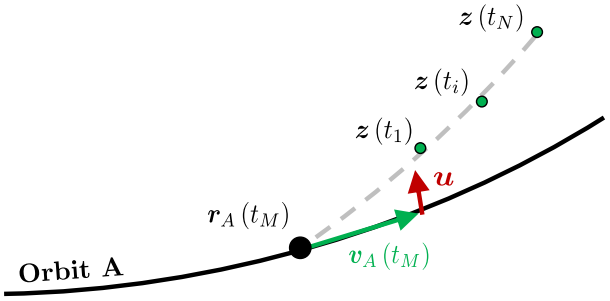

Figure 3: Sketch of the proposed track-to-orbit maneuver estimation problem.

Then, the maneuver magnitude, $\boldsymbol{u} \in \mathbb{R}^3$, for a given t_M, is estimated so that the residuals of the observations, $\boldsymbol{\rho}_i = \boldsymbol{z}(t_i) - \boldsymbol{h}(t_i, \boldsymbol{y}(t_i))$, difference between actual measurements and measurements reconstructed from the post-maneuver orbit, is minimized, i.e.:

$$J = \frac{1}{N} \sum_{i=1}^{N} \boldsymbol{\rho}_i^T \boldsymbol{W}_i \boldsymbol{\rho}_i \tag{4}$$

being $\boldsymbol{W}$ the weighting matrix, which contains the expected variance of each measurement. The solution can be obtained via a weighted non-linear least-squares method. To do so, the problem is linearized around a reference point, $\boldsymbol{u}_0$, and the corresponding correction, $\Delta\boldsymbol{u}$, is obtained by solving the following linear system:

$$\left(\boldsymbol{G}^T \boldsymbol{W} \boldsymbol{G}\right) \Delta\boldsymbol{u} = \left(\boldsymbol{G}^T \boldsymbol{W}\right) \Delta\boldsymbol{z} \tag{5}$$

where $\boldsymbol{G}$ is the Jacobian, i.e.: partials of the measurements with respect to the estimated parameters. This expression is similar to the classical orbit determination problem: $\left(\boldsymbol{H}^T \boldsymbol{W} \boldsymbol{H}\right) \Delta\boldsymbol{y} = \left(\boldsymbol{H}^T \boldsymbol{W}\right) \Delta\boldsymbol{z}$ [25], in which the residuals are minimized, being $\boldsymbol{H}$ the Jacobian in this case (partials of the measurements with respect to the state vector). In the problem at hand the Jacobian $\boldsymbol{G}$ is computed with respect to the parameters of the single burn maneuver $\boldsymbol{u}$ as opposed to $\boldsymbol{y}$ in $\boldsymbol{H}$.

Note that the state vector at each observation epoch, corresponding to the post-maneuver orbit and required for the evaluation of the Jacobian and residuals, can be linearly propagated by means of Equation 3.

Starting from a null initial solution and iteratively solving Equation 5 it is possible to obtain an estimation for $\Delta\boldsymbol{u}$. The Jacobian should be updated at each iteration to ensure convergence. Then, the contribution

Copyright © 2020 Advanced Maui Optical and Space Surveillance Technologies Conference (AMOS) – www.amostech.com

to $\boldsymbol{G}$ of the i^{th} observation is:

$$\boldsymbol{G}_i = \frac{\partial \boldsymbol{h}\left(t_i, \boldsymbol{y}_B\left(t_i\right)\right)}{\partial \boldsymbol{u}} = \frac{\partial \boldsymbol{h}\left(t_i, \boldsymbol{x}_B\left(t_i\right)\right)}{\partial \boldsymbol{y}_B\left(t_i\right)} \frac{\partial \boldsymbol{y}_B\left(t_i\right)}{\partial \boldsymbol{y}_B\left(t_M\right)} \frac{\partial \boldsymbol{y}_B\left(t_M\right)}{\partial \boldsymbol{u}} = \boldsymbol{H}_i \boldsymbol{\Psi}\left(t_i, t_M\right) \tag{6}$$

In order to detect the maneuver, the least-squares problem must be solved for a range of t_M values. In principle, the maneuver is assumed to have occurred after t_A^+, the epoch of the last observation considered for the estimation of the pre-maneuver orbit, and t_1, the epoch of the first available new observation. This thus makes it desirable to have a very computationally efficient estimation method, which is the rationale behind using a linearized post-maneuver orbit propagation, rather than a full numerical one.

Finally, a set of estimations $\{\boldsymbol{u}_k\}$ and corresponding objective function values $\{J_k\}$ for each $t_k \in \mathcal{T}$ for which the problem could be solved are to be obtained. Since the final goal of the maneuver estimation problem presented is the track-to-orbit association, we suggest taking every local minima of J and then selecting the solution as the one leading to minimum $|\boldsymbol{u}|$ (where $|\cdot|$ denotes the Euclidean norm when applied to a vector). Additional constraints can be included, such as introducing a u_{max} value to avoid the consideration of unrealistic maneuvers. Moreover, the n solutions leading to minimum $|\boldsymbol{u}|$ can be retained for a MHT approach. The complete method is summarized in Algorithm 1, where hat denotes estimated values.

Algorithm 1 Track-to-orbit (single burn) method

Require: $\boldsymbol{y}_A$ and $\boldsymbol{z}_i$ for $i = 1, \ldots, N$
1: **for** $t_M \in \mathcal{T} = \left[t_A^+, t_1\right]$ **do** ▷ Loop on maneuver epoch
2: Initial solution: $\boldsymbol{u} = \boldsymbol{0}$
3: Estimate $\boldsymbol{u}$ that minimizes the residuals (Equation 5)
4: **end for**
5: Locate J local minima in $\mathcal{T}$
6: Discard solutions with $|\hat{\boldsymbol{u}}| > u_{max}$
7: Sort remaining solutions according to $|\hat{\boldsymbol{u}}|$

2.2 Multiple burn maneuver detection and estimation via orbit-to-orbit

In this case we assume both the pre-maneuver orbit, $\boldsymbol{y}_A$, and the post-maneuver orbit, $\boldsymbol{y}_B$. This orbit-to-orbit check needs to be done before publishing the second orbit in the catalog to avoid duplicated objects.

The problem is then to find the transfer orbit, $\boldsymbol{x}_T$, that connects the pre-maneuver and post-maneuver orbits, i.e.:

$$\begin{cases} \boldsymbol{0} & = \boldsymbol{r}_T\left(t_{M1}\right) - \boldsymbol{r}_A\left(t_{M1}\right) \\ \boldsymbol{u}_1 & = \boldsymbol{v}_T\left(t_{M1}\right) - \boldsymbol{v}_A\left(t_{M1}\right) \end{cases} \tag{7}$$

$$\begin{cases} \boldsymbol{0} & = \boldsymbol{r}_B\left(t_{M2}\right) - \boldsymbol{r}_T\left(t_{M2}\right) \\ \boldsymbol{u}_2 & = \boldsymbol{v}_B\left(t_{M2}\right) - \boldsymbol{v}_T\left(t_{M2}\right) \end{cases} \tag{8}$$

where $\boldsymbol{u}_i$ represents the the i^{th} burn, i.e., delta-V, to be estimated.

The problem, illustrated in Figure 4 can be solved for $t_{M1}, t_{M2} \in \mathcal{T}$ such that $t_A^+ < t_{M1}$ (i.e.: the first burn occurs after the last observation used in the estimation of the pre-maneuver orbit) and $t_{M1} < t_{M2} < t_B^-$ (i.e., the second burn takes place after the first burn and prior to the first observation used in the estimation of the post-maneuver orbit).

Although the solution could be determined by solving Lambert's problem between $\boldsymbol{r}_A\left(t_{M1}\right)$ and $\boldsymbol{r}_B\left(t_{M2}\right)$ and then recovering the maneuver magnitudes directly from Equation 7 and Equation 8, we propose a method that uses linearized dynamics to propagate the effect of the maneuvers (as perturbations) in the orbits. This way, we avoid the limitation of the two-body motion dynamical model (i.e. Kepler's law) by considering

Copyright © 2020 Advanced Maui Optical and Space Surveillance Technologies Conference (AMOS) – www.amostech.com

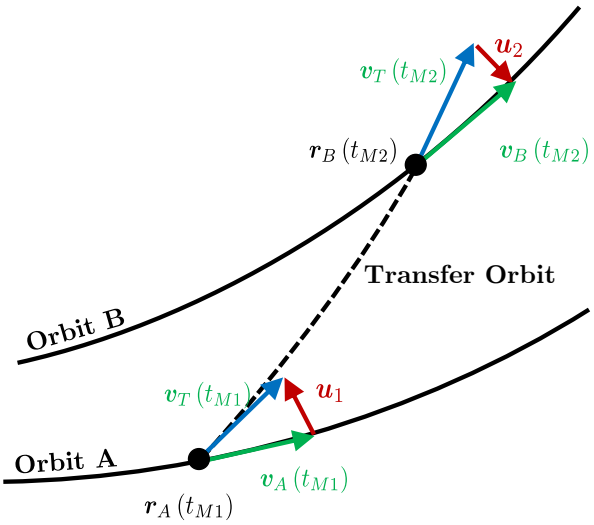

Figure 4: Sketch of the proposed orbit-to-orbit maneuver estimation problem.

relevant perturbations while keeping the computational effort low. Two equations arise from the propagation of the pre-maneuver and post-maneuver orbits, respectively:

$$\boldsymbol{x}_T\,(t) = \boldsymbol{x}_A\,(t) + \boldsymbol{\Phi}_{A,xv}\,(t, t_{M1})\,\boldsymbol{u}_1 \tag{9}$$

$$\boldsymbol{x}_T\,(t) = \boldsymbol{x}_B\,(t) - \boldsymbol{\Phi}_{B,xv}\,(t, t_{M2})\,\boldsymbol{u}_2 \tag{10}$$

A determined linear system can be constructed by using the linearized dynamics of the pre-maneuver orbit (A):

$$\begin{bmatrix} \boldsymbol{A}_{rv} & \boldsymbol{0} \\ \boldsymbol{A}_{vv} & \boldsymbol{I} \end{bmatrix} \cdot \begin{Bmatrix} \boldsymbol{u}_1 \\ \boldsymbol{u}_2 \end{Bmatrix} = \begin{Bmatrix} \boldsymbol{\Delta}_{2,r} \\ \boldsymbol{\Delta}_{2,v} \end{Bmatrix} \tag{11}$$

with:

$$\boldsymbol{A}_{\alpha\beta} = \frac{\partial \boldsymbol{\alpha}_A\,(t_{M2})}{\partial \boldsymbol{\beta}_A\,(t_{M1})} = \boldsymbol{\Phi}_{A,\alpha\beta}\,(t_{M2}, t_{M1}) \tag{12}$$

$$\boldsymbol{\Delta}_{k,\alpha} = \boldsymbol{\alpha}_B\,(t_{Mk}) - \boldsymbol{\alpha}_A\,(t_{Mk}) \tag{13}$$

Analogously, a determined linear system can be constructed by using the linearized dynamics of the post-maneuver orbit (B):

$$\begin{bmatrix} \boldsymbol{0} & \boldsymbol{B}_{rv} \\ \boldsymbol{I} & \boldsymbol{B}_{vv} \end{bmatrix} \cdot \begin{Bmatrix} \boldsymbol{u}_{1,v} \\ \boldsymbol{u}_{2,v} \end{Bmatrix} = \begin{Bmatrix} \boldsymbol{\Delta}_{1,r} \\ \boldsymbol{\Delta}_{1,v} \end{Bmatrix} \tag{14}$$

with:

$$\boldsymbol{B}_{\alpha\beta} = \frac{\partial \boldsymbol{\alpha}_B\,(t_{M2})}{\partial \boldsymbol{\beta}_B\,(t_{M1})} = \boldsymbol{\Phi}_{B,\alpha\beta}\,(t_{M2}, t_{M1}) \tag{15}$$

Copyright © 2020 Advanced Maui Optical and Space Surveillance Technologies Conference (AMOS) – www.amostech.com

Although either Equation 11 or Equation 14 could be directly solved to obtain $\boldsymbol{u}_1$ and $\boldsymbol{u}_2$, we suggest combining the two linear systems to obtain the following problem:

$$\begin{bmatrix} \boldsymbol{0} & \boldsymbol{B}_{rv} \\ \boldsymbol{I} & \boldsymbol{B}_{vv} \\ \boldsymbol{A}_{rv} & \boldsymbol{0} \\ \boldsymbol{A}_{vv} & \boldsymbol{I} \end{bmatrix} \cdot \begin{Bmatrix} \boldsymbol{u}_1 \\ \boldsymbol{u}_2 \end{Bmatrix} = \begin{Bmatrix} \boldsymbol{\Delta}_{1,r} \\ \boldsymbol{\Delta}_{1,v} \\ \boldsymbol{\Delta}_{2,r} \\ \boldsymbol{\Delta}_{2,v} \end{Bmatrix} \tag{16}$$

The solution of this overdetermined system (12 equations, 6 unknowns) can be obtained via least-squares, i.e., by solving the following linear system:

$$\left(\boldsymbol{X}^T \boldsymbol{X}\right) \boldsymbol{u} = \boldsymbol{X}^T \boldsymbol{\Delta} \tag{17}$$

where $\boldsymbol{X}$ is the left-hand-side matrix and $\boldsymbol{\Delta}$ the right-hand-side vector in Equation 16. $\boldsymbol{u} = \{\boldsymbol{u}_1, \boldsymbol{u}_2\}^T$ can be solved with any factorization method such as Cholesky decomposition.

Since this method is based on a linearization of the dynamics of the two orbits, there is an inherent applicability limitation related to the magnitude of the perturbations above which the linear dynamics assumption is expected to fail. Therefore, the most limiting use case is expected to be the estimation of maneuvers in the velocity direction (along-track), given that it is the main direction of the dynamics (greater effect of perturbations).

The solution of Equation 16 is expected to be a smooth combination of the two dynamics. Moreover, note that the contribution of each orbit could be weighted if required with a confidence level or covariance, for instance. The complete method is summarized in Algorithm 2.

Algorithm 2 Orbit-to-orbit (multiple burn) method

Require: $\boldsymbol{y}_A$ and $\boldsymbol{y}_B$
1: **for** $t_{M1}, t_{M2} \in \mathcal{T} = \left[t_A^+, t_{M2}\right] \times \left[t_{M1}, t_B^-\right]$ **do** ▷ Loop on maneuver epoch
2: Solve overdetermined linear problem (Equation 16)
3: **end for**
4: Discard solutions with $|\hat{\boldsymbol{u}}| > u_{max}$
5: Sort remaining solutions according to $|\hat{\boldsymbol{u}}|$

3. RESULTS

The track-to-orbit and orbit-orbit methods, presented in Section 2, have been applied to scenarios with simulated and real observations.

Regarding the track-to-orbit scenarios, the pre-maneuver orbit is estimated by using the observations available before the maneuver via a batch least-squares orbit determination and propagated to the future to cover the post-maneuver tracks. Then, the post-maneuver tracks are associated incrementally via track-to-track association [18] and finally, the track-to-orbit method, presented in Section 2.1, is applied to each pair of pre-maneuver orbit and post-maneuver track associations. The sequence of events is depicted in Figure 5.

In the case of the orbit-to-orbit scenarios, the pre-maneuver and post-maneuver orbits are estimated analogously, by means of an orbit determination with the observations available before and after, respectively. Then, the orbit-to-orbit method, presented in Section 2.2, is applied to the pair orbits. The sequence of events is depicted in Figure 6.

The dynamical model considered for the state propagation, typical in the case of GEO, consists in a 30x30 Earth gravitational field, Moon and Sun third body perturbations and cannonball model for the Solar Radiation Pressure (SRP).

Copyright © 2020 Advanced Maui Optical and Space Surveillance Technologies Conference (AMOS) – www.amostech.com

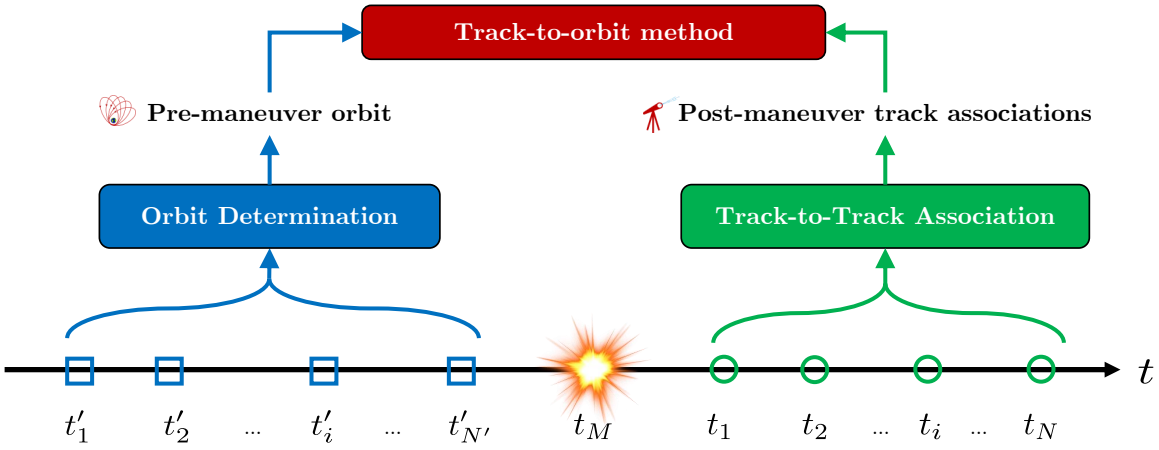

Figure 5: Sequence of events in track-to-orbit scenarios.

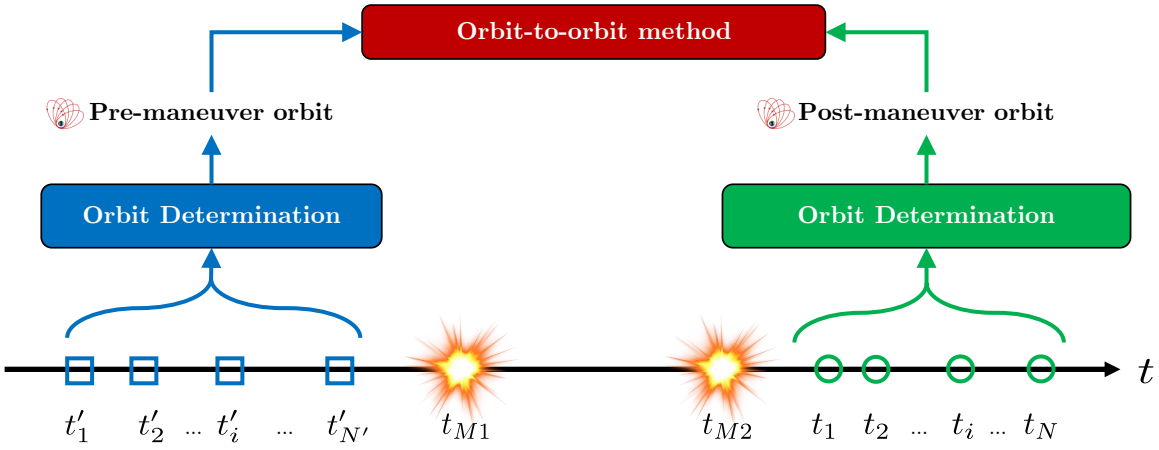

Figure 6: Sequence of events in orbit-to-orbit scenarios.

3.1 Track-to-orbit: simulated observations

The first assessment of the track-to-orbit methodology is aimed at investigating the impact of the number of tracks and perform a preliminary analysis of the method under a simulated scenario. To do so, an initial state vector was propagated from t_0 up to $t_0 + 7$ days considering an impulsive maneuver in the local RIC frame (Radial, In-track, Cross-track) at the middle of the interval. This orbit will be referred to as *reference orbit* and three cases have been studied: 1) radial burn, 2) in-track burn and 3) cross-track burn. The magnitude of the maneuver is $|\boldsymbol{u}|\, u = 1.0\, m/s$ for each case.

On the one hand, a pre-maneuver orbit was generated by performing the same propagation as the reference orbit but without considering the maneuver. On the other hand, an optical sensor station was simulated to receive three tracks on the 5th day (12 hours after the maneuver), 6th day (36 hours after the maneuver) and 7th day (60 hours after the maneuver). Each track starts at t_i^-, has a duration of $t_i^+ - t_i^- = 15\, min$ and contains an observation (pair of right ascension, α, and declination, δ) every 8 s. Gaussian noise with zero-mean and $\sigma_\alpha = \sigma_\delta$ has been added to the simulated measurements. The details of this preliminary case are summarized in Table 1.

The problem was solved for $t_M \in \left[t_0, t_1^-\right]$ and for each possible combination of the three tracks, i.e.: $\{1\}$, $\{2\}$, $\{3\}$, $\{1,2\}$, $\{1,3\}$, $\{2,3\}$ and $\{1,2,3\}$, following the method presented in Section 2.1, aimed at minimizing

Copyright © 2020 Advanced Maui Optical and Space Surveillance Technologies Conference (AMOS) – www.amostech.com

Table 1: Initial state vector, maneuver epoch and available tracks information of the track-to-orbit simulated scenario.

Parameter	Value	Units
t_0	2009/01/01-00:00	
a	42192.17	km
e	$2.71{\cdot}10^{-4}$	
i	13.72	deg
Ω	12.21	deg
ω	317.51	deg
ν	227.82	deg
$C_R A/m$	0.015	m^2/kg
t_M	2009/01/04-12:00	
t_1^-	2009/01/05 00:00	
t_2^-	2009/01/06 00:00	
t_3^-	2009/01/07 00:00	
$t_i^+ - t_i^-$	15.0	min
$\sigma_\alpha = \sigma_\delta$	1.0	arcsec

$\sqrt{J}$ by the addition of a maneuver. Figure 7, Figure 8 and Figure 9 show $|\hat{\boldsymbol{u}}|$ (red) and $\sqrt{J}$ (purple) for the radial, in-track and cross-track maneuver cases, respectively, and three tracks (hat denotes estimated values). The red horizontal dotted line represents the true magnitude of the maneuver and the black vertical dotted line the true maneuver epoch. There are several local minima on $|\hat{\boldsymbol{u}}|$ and $\sqrt{J}$ that not always coincide, with a time separation of around 1 day, which is the orbital period. This non-linear behavior is precisely what suggested us that a joint estimation of both the maneuver epoch and magnitude may not be a right choice, at least for an initial maneuver estimation approach.

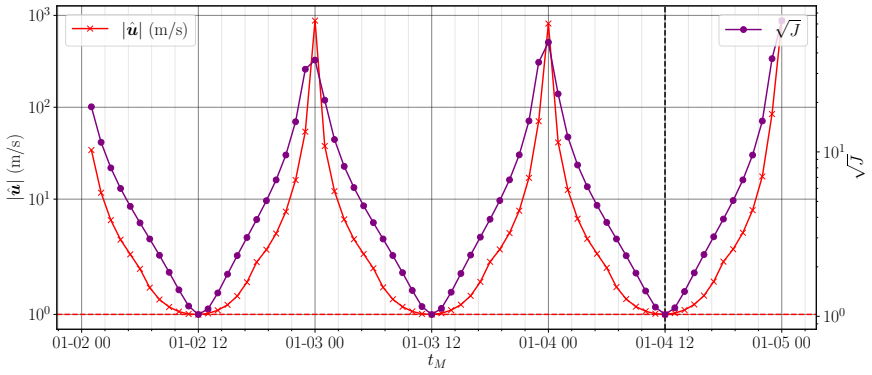

Figure 7: $|\hat{\boldsymbol{u}}|$ and $\sqrt{J}$ variation with maneuver time for the track-to-orbit simulated radial burn and tracks $\{1, 2, 3\}$.

The details of each $\sqrt{J}$ local minima is compiled in Table 2, where apart from the maneuver estimation results, the errors in the semi-major axis, eccentricity and inclination estimations (corresponding to the pre-maneuver orbit after the application of the estimated maneuver) are also shown. It is clear how the solution with lowest $|\hat{\boldsymbol{u}}|$ corresponds to the truth, which is also the solution with lowest orbital difference with respect to the reference orbit.

Note that cases involving tracks $\{1, 2, 3\}$ are the best conditioned ones since three tracks are involved. Figure 10 shows the $|\hat{\boldsymbol{u}}|$ and $\sqrt{J}$ distribution of the $\sqrt{J}$ local minima found for each combination of tracks, along the semi-major axis and eccentricity errors in the radial burn case. Although several $\sqrt{J}$ local minima are found when considering only a single track, even with $|\hat{\boldsymbol{u}}| \sim 1m/s$ and $\sqrt{J} \sim 1$, more information (tracks)

Copyright © 2020 Advanced Maui Optical and Space Surveillance Technologies Conference (AMOS) – www.amostech.com

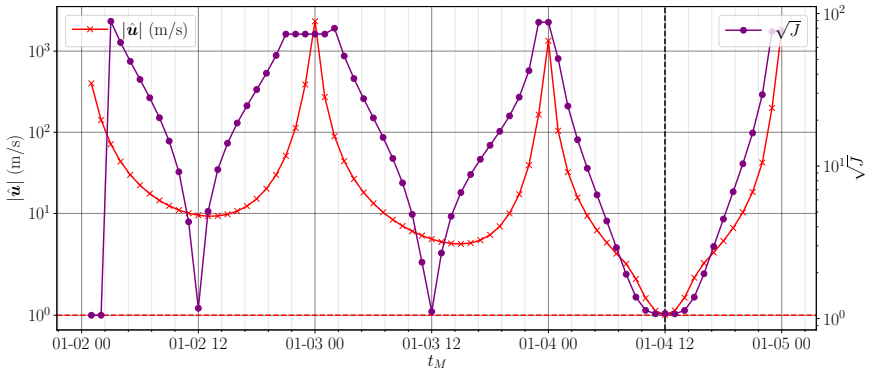

Figure 8: $|\hat{\boldsymbol{u}}|$ and $\sqrt{J}$ variation with maneuver time for the track-to-orbit simulated in-track burn and tracks $\{1, 2, 3\}$.

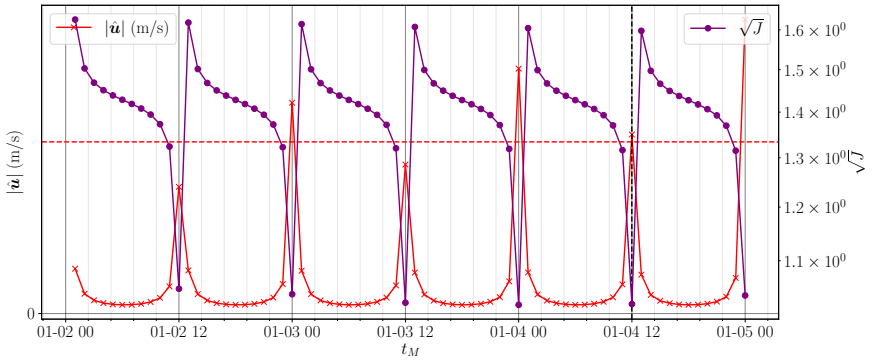

Figure 9: $|\hat{\boldsymbol{u}}|$ and $\sqrt{J}$ variation with maneuver time for the track-to-orbit simulated cross-track burn and tracks $\{1, 2, 3\}$.

Table 2: Details of each $\sqrt{J}$ local minima for the track-to-orbit simulated scenario with association of tracks $\{1, 2, 3\}$.

case	t_M	$\sqrt{J}$	$\hat{u}_R$ (m/s)	$\hat{u}_I$ (m/s)	$\hat{u}_C$ (m/s)	$\lvert\hat{\boldsymbol{u}}\rvert$ (m/s)	$\hat{a} - a$ (km)	$\hat{e} - e$	$\hat{i} - i$ (deg)
Radial burn	2009/01/02-12:00	1.0258	0.9964	0.0003	0.0339	0.9970	0.8617	$7.88 \cdot 10^{-6}$	$1.40 \cdot 10^{-3}$
($u_R = 1\,m/s$)	2009/01/03-12:00	1.0250	0.9988	0.0002	0.0347	0.9994	0.3586	$1.50 \cdot 10^{-6}$	$6.09 \cdot 10^{-4}$
	2009/01/04-12:00	1.0247	1.0012	0.0002	0.0349	1.0018	0.0045	$1.05 \cdot 10^{-6}$	$6.44 \cdot 10^{-4}$
In-track burn	2009/01/02-12:00	1.1686	-9.4404	0.8948	-0.1174	9.4835	3.4345	$1.99 \cdot 10^{-3}$	$4.20 \cdot 10^{-3}$
	2009/01/03-12:00	1.1105	-4.7165	0.9757	-0.0031	4.8163	0.9697	$6.04 \cdot 10^{-4}$	$1.31 \cdot 10^{-3}$
($u_I = 1\,m/s$)	2009/01/04-11:00	1.0740	-0.4572	0.9991	0.0155	1.0988	0.0343	$1.96 \cdot 10^{-5}$	$1.33 \cdot 10^{-4}$
	2009/01/04-13:00	1.0730	0.4697	0.9979	-0.0204	1.1031	0.2660	$8.20 \cdot 10^{-7}$	$2.57 \cdot 10^{-4}$
Cross-track burn	2009/01/02-12:00	1.0511	0.0009	-0.0002	0.7383	0.7383	0.8719	$1.27 \cdot 10^{-5}$	$6.83 \cdot 10^{-3}$
	2009/01/03-00:00	1.0418	-0.9289	-0.0006	-0.8035	1.2282	0.7575	$1.97 \cdot 10^{-4}$	$5.34 \cdot 10^{-3}$
	2009/01/03-12:00	1.0275	0.0011	-0.0002	0.8681	0.8681	0.3685	$4.38 \cdot 10^{-6}$	$3.66 \cdot 10^{-3}$
($u_C = 1\,m/s$)	2009/01/04-00:00	1.0239	-1.0640	-0.0007	-0.9505	1.4268	0.4169	$2.57 \cdot 10^{-4}$	$1.62 \cdot 10^{-3}$
	2009/01/04-12:00	1.0253	0.0013	-0.0003	1.0428	1.0428	0.0050	$2.06 \cdot 10^{-6}$	$7.91 \cdot 10^{-4}$

is required to reliably estimate the effect of the maneuver on the orbit. Only when two and three tracks are involved, solutions with $|a - \hat{a}| < 10\,m$ and $|e - \hat{e}| < 10^{-5}$ are found and the local minima converge to the truth.

Copyright © 2020 Advanced Maui Optical and Space Surveillance Technologies Conference (AMOS) – www.amostech.com

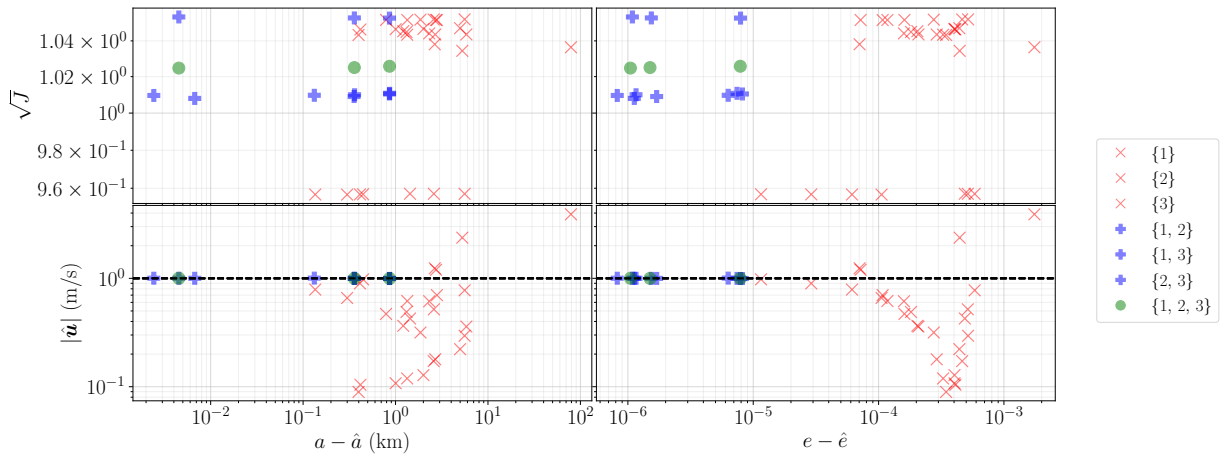

Figure 10: $|\boldsymbol{u}|$ and $\sqrt{J}$ distribution of the $\sqrt{J}$ local minima found for each combination of tracks in the track-to-orbit simulated radial burn case.

3.2 Orbit-to-orbit: simulated observations

The first assessment of the orbit-to-orbit methodology is aimed at performing a preliminary analysis of the method and comparison against Lambert's problem solution. To do so, an initial state vector was propagated from t_0 up to $t_0 + 7$ days considering two impulsive maneuvers in the local RIC frame. As in Section 3.1, this orbit will be referred to as *reference orbit* and six cases have been studied: 1) two radial burns (RR), 2) two in-track burns (II), 3) two cross-track burns (CC), 4) radial and in-track burns (RI), 5) radial and cross-track burns (RC) and 6) in-track and cross-track (IC) burns. The magnitude of the maneuvers are $\boldsymbol{u}_1 = +0.1\boldsymbol{e}_i\, m/s$ and $\boldsymbol{u}_2 = -0.1\boldsymbol{e}_i\, m/s$, being $\boldsymbol{e}_i$ the unitary vector in the R, I or C direction, i.e.: the sense of the first burn is positive, while the one of the second is negative with respect to the RIC frame. The first burn is simulated at $t_{M1} = 2009/01/03 - 12:00$ and the second burn at $t_{M2} = 2009/01/04 - 12:00$.

On the one hand, the pre-maneuver orbit was generated by performing the same propagation as the reference orbit but without considering the maneuvers. On the other hand, the post-maneuver orbit was generated by performing a back-propagation of the last state vector of the reference orbit without considering the maneuvers. The initial state vector is the same as in the track-to-orbit simulated scenario (Table 1).

In this case, the outcome of the maneuver estimation method are the two estimated burns, $\hat{\boldsymbol{u}}_1$ and $\hat{\boldsymbol{u}}_2$, for each $\hat{t}_{M1}$ and $\hat{t}_{M2}$ in the mesh used to sample $\mathcal{T}$. Figure 11 shows the distribution of the total velocity increase, i.e.: $|\hat{\boldsymbol{u}}_1| + |\hat{\boldsymbol{u}}_2|$, along $\left[\hat{t}_{M1}, \hat{t}_{M2}\right] \in \mathcal{T}$ in the II (left) and RI (right) cases. Note that solutions with $|\hat{\boldsymbol{u}}| > 5\, m/s$ have been discarded. This representation, known as porkchop plot, provides the velocity increase required for each combination of $\hat{t}_{M1}$ and $\hat{t}_{M2}$ that connects the pre-maneuver and post-maneuver orbits. Since there are no metrics to select a candidate estimation besides the maneuver magnitude, the optimal maneuver, i.e. minimum $|\hat{\boldsymbol{u}}| = |\hat{\boldsymbol{u}}_1| + |\hat{\boldsymbol{u}}_2|$ is accepted as solution. However, in Figure 11, the presence of multiple local minima confirms the existence of maneuvers with similar control effort that connect the two orbits. In principle, they are equivalent from the association point of view, meaning that an accurate estimation of the maneuver epoch cannot be ensured.

The three lowest $|\hat{\boldsymbol{u}}|$ of each case are presented in Table 3. In most cases, the corresponding $\hat{t}_{M1}$ and $\hat{t}_{M2}$ do not match the true values and $|\hat{\boldsymbol{u}}| < |\boldsymbol{u}|$, meaning that a more optimal maneuver than the true one has been found. The norm of the overdetermined linear system, ϵ, suggests that the linear system has been properly solved.

In order to evaluate the accuracy of the estimations, the estimated maneuvers magnitude at t_{M1} and t_{M2} (true values) for each case is summarized in Table 4.

Finally, the performance of the proposed method against classical Lambert's problem was investigated. Figure 12 depicts the distribution of $|\hat{\boldsymbol{u}}_1| + |\hat{\boldsymbol{u}}_2|$ along the time of flight, $\hat{t}_{M2} - \hat{t}_{M1}$, as provided by the

Copyright © 2020 Advanced Maui Optical and Space Surveillance Technologies Conference (AMOS) – www.amostech.com

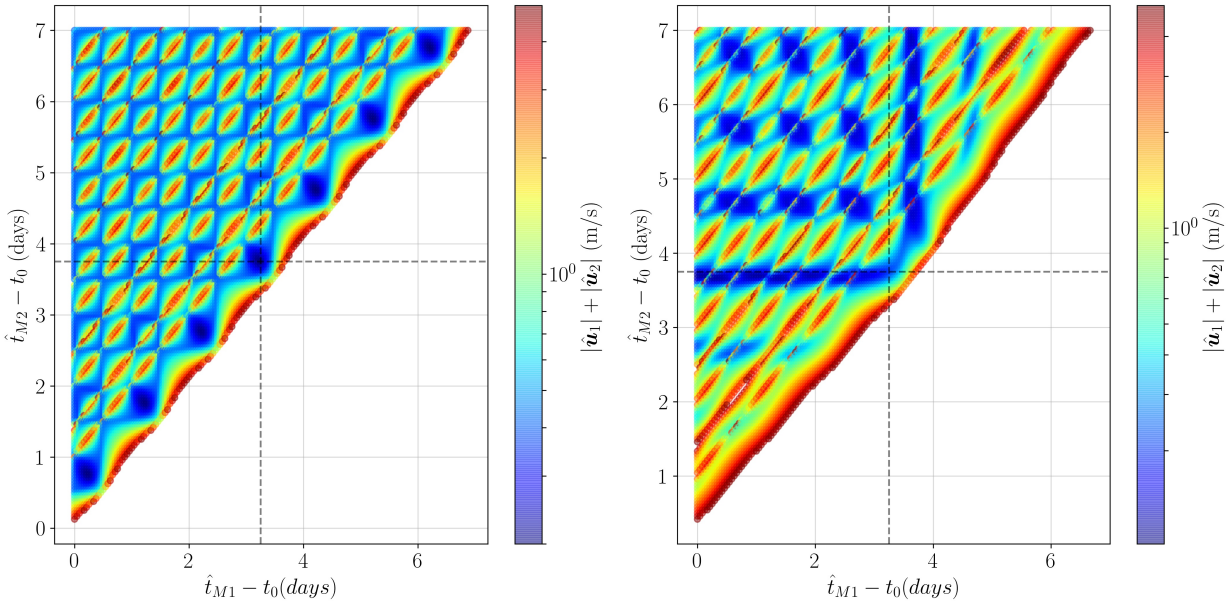

Figure 11: Porkchop plots for the orbit-to-orbit simulated *II* (left) and *RI* (right) cases.

Table 3: Three lowest $|\hat{\boldsymbol{u}}|$ of each orbit-to-orbit simulated case.

case	$\hat{t}_{M1}$	$\hat{t}_{M2}$	ϵ (m/s)	$\lvert\hat{\boldsymbol{u}}_1 - \boldsymbol{u}_1\rvert$ (m/s)	$\lvert\hat{\boldsymbol{u}}_2 - \boldsymbol{u}_2\rvert$ (m/s)	$\lvert\hat{\boldsymbol{u}} - \boldsymbol{u}\rvert$
RR	2009/01/01-00:00	2009/01/01-17:00	$1.54 \cdot 10^{-15}$	0.02249	0.14996	0.17245
	2009/01/07-07:00	2009/01/08-00:00	$1.55 \cdot 10^{-15}$	0.14998	0.02248	0.17247
	2009/01/01-12:00	2009/01/02-05:00	$1.50 \cdot 10^{-15}$	0.02229	0.15047	0.17276
II	2009/01/04-06:00	2009/01/04-18:00	$1.75 \cdot 10^{-13}$	0.09997	0.09997	0.19994
	2009/01/05-06:00	2009/01/05-18:00	$1.76 \cdot 10^{-13}$	0.10000	0.09999	0.19999
	2009/01/03-06:00	2009/01/03-18:00	$1.74 \cdot 10^{-13}$	0.10001	0.10000	0.20001
CC	2009/01/03-18:00	2009/01/04-18:00	$1.67 \cdot 10^{-17}$	0.05570	0.14426	0.19995
	2009/01/02-18:00	2009/01/04-18:00	$4.42 \cdot 10^{-17}$	0.02785	0.17210	0.19996
	2009/01/01-18:00	2009/01/04-18:00	$5.63 \cdot 10^{-17}$	0.01858	0.18138	0.19996
RI	2009/01/03-12:00	2009/01/07-23:00	$6.41 \cdot 10^{-08}$	0.06567	0.03608	0.10175
	2009/01/01-03:00	2009/01/04-17:00	$4.44 \cdot 10^{-10}$	0.00538	0.10803	0.11341
	2009/01/01-04:00	2009/01/04-17:00	$6.17 \cdot 10^{-10}$	0.00723	0.10652	0.11376
RC	2009/01/06-19:00	2009/01/07-16:00	$8.57 \cdot 10^{-15}$	0.08623	0.05103	0.13726
	2009/01/05-19:00	2009/01/06-16:00	$8.58 \cdot 10^{-15}$	0.08811	0.04916	0.13727
	2009/01/04-19:00	2009/01/05-16:00	$8.59 \cdot 10^{-15}$	0.08997	0.04731	0.13728
IC	2009/01/02-21:00	2009/01/04-06:00	$5.89 \cdot 10^{-11}$	0.00087	0.14052	0.14139
	2009/01/01-21:00	2009/01/04-06:00	$1.47 \cdot 10^{-10}$	0.00088	0.14067	0.14155
	2009/01/04-06:00	2009/01/06-20:00	$9.74 \cdot 10^{-11}$	0.14042	0.00115	0.14158

proposed orbit-to-orbit method (blue) and Lambert's problem solution (red) in the case of two in-track burns. It is clear how there is a divergence of the solutions as the time of flight increases, due to the orbit dynamics mismodelling of the Lambert's problem solution (two-body motion), noticeable for $\hat{t}_{M2} - \hat{t}_{M1} > 1\,day$. This justifies the choice of the linearized orbit model including perturbations over a two-body motion model.

Copyright © 2020 Advanced Maui Optical and Space Surveillance Technologies Conference (AMOS) – www.amostech.com

Table 4: Error in the estimation of $|\boldsymbol{u}_1|$ and $|\boldsymbol{u}_2|$ for the orbit-to-orbit simulated cases.

case	ϵ	$\lvert\hat{\boldsymbol{u}}_1 - \boldsymbol{u}_1\rvert$ (m/s)	$\lvert\hat{\boldsymbol{u}}_2 - \boldsymbol{u}_2\rvert$ (m/s)	$\lvert\hat{\boldsymbol{u}} - \boldsymbol{u}\rvert$ (m/s)
RR	$3.05 \cdot 10^{-15}$	$1.15 \cdot 10^{-05}$	$1.15 \cdot 10^{-05}$	$1.00 \cdot 10^{-08}$
II	$1.75 \cdot 10^{-13}$	$2.81 \cdot 10^{-05}$	$2.81 \cdot 10^{-05}$	$5.62 \cdot 10^{-05}$
CC	$3.84 \cdot 10^{-21}$	$3.00 \cdot 10^{-08}$	$7.00 \cdot 10^{-08}$	$4.00 \cdot 10^{-08}$
RI	$6.87 \cdot 10^{-14}$	$1.15 \cdot 10^{-05}$	$2.81 \cdot 10^{-05}$	$1.66 \cdot 10^{-05}$
RC	$1.45 \cdot 10^{-15}$	$1.15 \cdot 10^{-05}$	$7.00 \cdot 10^{-08}$	$1.16 \cdot 10^{-05}$
IC	$6.24 \cdot 10^{-14}$	$2.81 \cdot 10^{-05}$	$7.00 \cdot 10^{-08}$	$2.80 \cdot 10^{-05}$

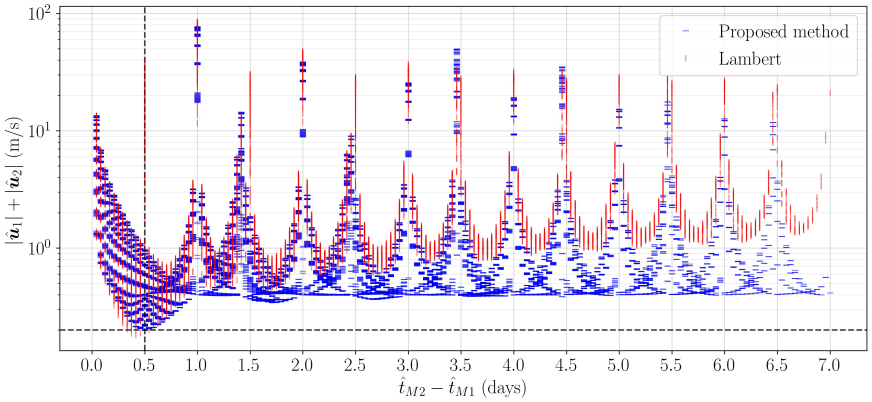

Figure 12: Distribution of $|\hat{\boldsymbol{u}}_1| + |\hat{\boldsymbol{u}}_2|$ along $\hat{t}_{M2} - \hat{t}_{M1}$ for the orbit-to-orbit simulated *II* case.

3.3 Track-to-orbit: real observations

Once the performance of the track-to-orbit method with simulated data has been studied, a scenario with real observations was set up to confirm the adequacy of the proposed method. It consists in a real GEO satellite providing coverage to Europe and a telescope from the ISON network located in eastern Europe. The observations are distributed along two weeks and the maneuvers performed by the RSO are: 1) a North-South (NS) maneuver on $t_0 + 5\,days$ with $|\boldsymbol{u}| \sim 1.15\,m/s$, 2) an East-West (EW) maneuver on $t_0 + 7\,days$ with $|\boldsymbol{u}| \sim 0.5\,mm/s$. The sequence of events is shown in Table 5.

Table 5: Sequence of events in the real observations scenario.

Event	Epoch
NS burn	2016/04/12-06:42
Track #1	2016/04/12-23:11
Track #2	2016/04/13-00:39
Track #3	2016/04/13-01:44
Track #4	2016/04/13-19:19
Track #5	2016/04/13-20:11
EW burn	2016/04/14-20:17
Track #6	2016/04/15-19:28
Track #7	2016/04/16-19:10
Track #8	2016/04/16-21:19
Track #9	2016/04/16-21:58

Copyright © 2020 Advanced Maui Optical and Space Surveillance Technologies Conference (AMOS) – www.amostech.com

3.3.1 NS burn

Five tracks, $\{1,2,3,4,5\}$, were available after the first burn and before the second burn and associations of two and three tracks were used for the estimation of the maneuver. Figure 13 shows the variation of $\hat{u}_i$ and $\sqrt{J}$ with $\hat{t}_M$, for the pair formed by the pre-maneuver orbit and the association of tracks $\{1,3\}$. The horizontal dashed lines correspond to the true values of each maneuver component, while the vertical dashed line represents the real epoch of the maneuver and it is precisely a local minima of $\sqrt{J}$. However, there are two additional $\hat{u}_i$ local minima half orbital period before and after the true t_M. These correspond to different maneuvers that are compatible with the tracks considered and in fact they present similar $|\hat{\boldsymbol{u}}|$ values.

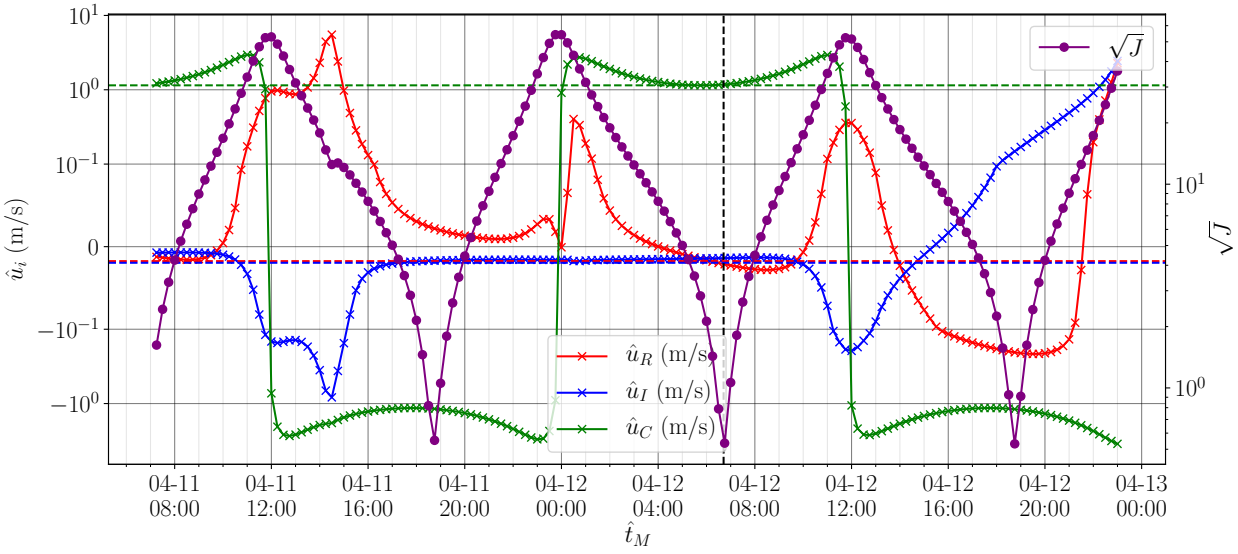

Figure 13: $\hat{u}_i$ and $\sqrt{J}$ variation along $\hat{t}_M$ for the track-to-orbit real NS maneuver and tracks $\{1,3\}$.

The local minima corresponding to each with $|\hat{\boldsymbol{u}}| < 2\,m/s$ are presented in Table 6. The estimations are consistent along the different track associations and a solution close to the true maneuver ($t_M = 04{-}1206:42$ and $|\hat{\boldsymbol{u}}| \sim 1.15\,m/s$) is found while $\sqrt{J} \sim 1$. Note that associating three tracks allows to discard a pair of local minima with $\sqrt{J} \sim 3.6$, while this is not possible if only association of two tracks are used.

Table 6: $|\hat{\boldsymbol{u}}|$ local minima found for each association of tracks in the track-to-orbit real NS maneuver scenario.

tracks	$\hat{t}_M$	$\sqrt{J}$	$\lvert\hat{\boldsymbol{u}}\rvert$ (m/s)	tracks	$\hat{t}_M$	$\sqrt{J}$	$\lvert\hat{\boldsymbol{u}}\rvert$ (m/s)	tracks	$\hat{t}_M$	$\sqrt{J}$	$\lvert\hat{\boldsymbol{u}}\rvert$ (m/s)
$\{1,2\}$	12-18:45:00	0.53	1.22	$\{2,3\}$	12-18:45	0.59	1.20	$\{3,5\}$	11-18:45	1.02	1.19
$\{1,2\}$	11-18:45:00	0.54	1.18	$\{2,3\}$	11-18:45	0.60	1.18	$\{3,5\}$	12-06:45	1.11	1.20
$\{1,2\}$	12-06:45:00	0.54	1.18	$\{2,3\}$	12-06:45	0.60	1.18	$\{3,5\}$	12-18:30	1.23	1.14
$\{1,3\}$	12-18:45:00	0.53	1.21	$\{2,4\}$	11-18:45	1.15	1.18	$\{4,5\}$	11-18:45	0.76	1.23
$\{1,3\}$	12-06:45:00	0.54	1.18	$\{2,4\}$	12-06:45	1.27	1.19	$\{4,5\}$	12-06:45	0.79	1.25
$\{1,3\}$	11-18:45:00	0.55	1.18	$\{2,4\}$	12-18:30	1.29	1.15	$\{4,5\}$	13-06:30	0.78	1.11
$\{1,4\}$	11-18:45:00	0.87	1.18	$\{2,5\}$	11-18:45	1.01	1.19	$\{1,3,4\}$	11-18:45	1.03	1.18
$\{1,4\}$	12-06:45:00	0.87	1.18	$\{2,5\}$	12-06:45	1.12	1.19	$\{1,3,4\}$	12-06:45	1.05	1.18
$\{1,4\}$	12-18:30:00	1.17	1.15	$\{2,5\}$	12-18:30	1.12	1.15	$\{1,3,4\}$	12-18:30	3.64	1.15
$\{1,5\}$	11-18:45:00	0.79	1.18	$\{3,4\}$	11-18:45	1.18	1.19	$\{1,3,5\}$	11-18:45	0.92	1.18
$\{1,5\}$	12-06:45:00	0.80	1.18	$\{3,4\}$	12-06:45	1.31	1.19	$\{1,3,5\}$	12-06:45	0.95	1.18
$\{1,5\}$	12-18:30:00	1.08	1.15	$\{3,4\}$	12-18:30	1.40	1.15	$\{1,3,5\}$	12-06:45	3.63	1.15

Copyright © 2020 Advanced Maui Optical and Space Surveillance Technologies Conference (AMOS) – www.amostech.com

3.3.2 EW burn

In this case four tracks, $\{6, 7, 8, 9\}$, were available after the second burn and again, associations of up to three tracks were used for the estimation of the maneuver. Figure 14 shows the distribution of every $|\boldsymbol{u}|$ local minima found along $|\boldsymbol{u}|$ and $\sqrt{J}$. Even though this case is more challenging that the previous NS maneuver due to the low $|\boldsymbol{u}|$ involved, which is translated into a fainter maneuver footprint on the residuals, associations of two and three tracks are able to estimate a burn within the order of magnitude of the truth.

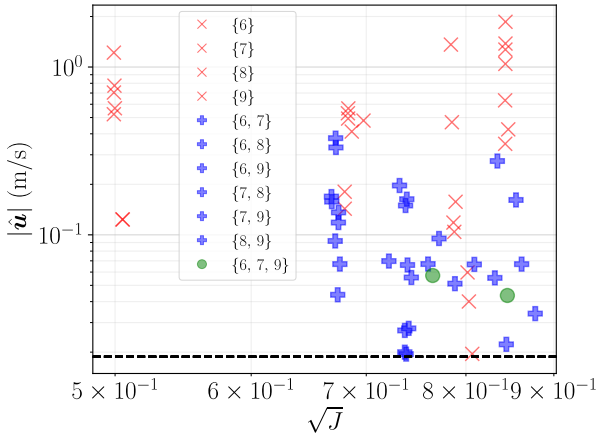

Figure 14: $|\boldsymbol{u}|$ and $\sqrt{J}$ distribution of the $\sqrt{J}$ local minima found for each combination of tracks in the real EW maneuver scenario.

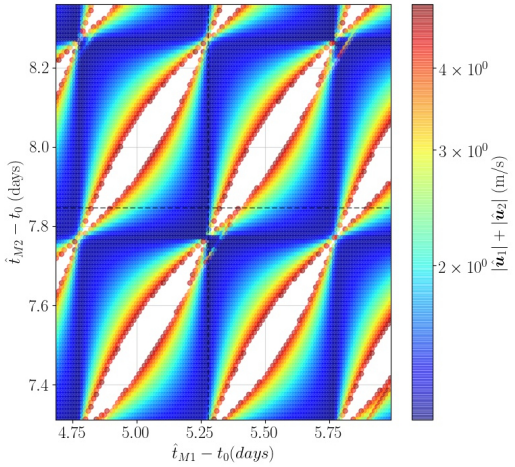

Figure 15: Porkchop plot zoom for the orbit-to-orbit real scenario.

3.4 Orbit-to-orbit: real observations

The same observations set used in Section 3.3 has been used to study the performance of the orbit-to-orbit method in a real scenario.

Figure 15 shows the resulting porkchop plot (zoomed in the vicinity of the true solution and discarding solutions with $|\hat{\boldsymbol{u}}| > 5\,m/s$) that as in the simulated scenario present many local minima corresponding to maneuvers able to link the two orbits. The total estimated maneuver magnitude at t_{M1} and t_{M2} is $|\hat{\boldsymbol{u}}| = 1.29\,m/s$, i.e., a relative error of less than 10%. Again, without additional information it is not possible to select a single solution since the local minima have similar values of $|\hat{\boldsymbol{u}}|$ and are able to solve the linkage problem. As a projection of this distribution on the $\hat{t}_2 - \hat{t}_1$ (time of flight) plane, in Figure 16, illustrates this fact and also justifies the suitability of defining a threshold u_{max} such that $|\hat{\boldsymbol{u}}| < u_{max}$ to reduce the number of solutions. In this case, there are a total of 96,141 solutions, which reduces to the 80% with $u_{max} = 5\,m/s$ and to 46% with $u_{max} = 2\,m/s$.

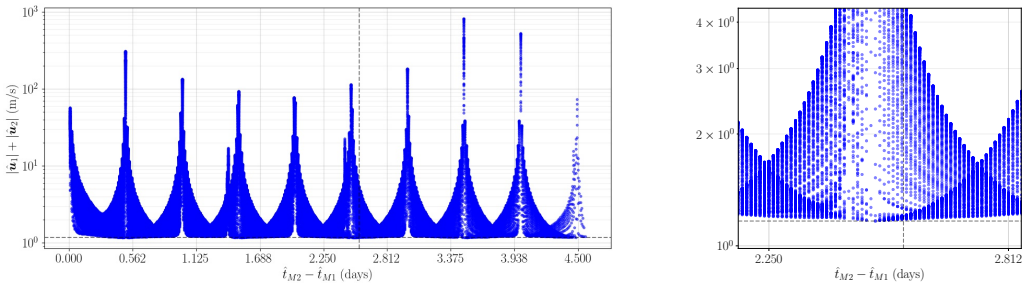

Figure 16: $|\hat{\boldsymbol{u}}_1| + |\hat{\boldsymbol{u}}_2|$ distribution along $\hat{t}_2 - \hat{t}_1$ for the orbit-to-orbit real scenario.

Copyright © 2020 Advanced Maui Optical and Space Surveillance Technologies Conference (AMOS) – www.amostech.com

Finally, Table 7 presents the four optimal solution (i.e.: lowest $|\hat{\boldsymbol{u}}|$). The true maneuver epochs are $t_{M1} = 04/12 - 06:42$ and $t_{M2} = 04/14 - 20:17$ and therefore $\left|\hat{t}_{M1} - t_{M1}\right| < 15\,min$ and $\left|\hat{t}_{M2} - t_{M2}\right| < 2\,h$ in the case of the optimal solution. Although this maneuver is different than the true one in terms of $|\hat{\boldsymbol{u}}_1|$ and $|\hat{\boldsymbol{u}}_2|$, if independently considered, the total velocity increase, $|\hat{\boldsymbol{u}} - \boldsymbol{u}|$ is estimated with an error lower than the 1.5% of the true value. This means that the goal of estimation two potential maneuvers whose $|\hat{\boldsymbol{u}}|$ is of the same order of magnitude of the real one is achieved.

Table 7: $|\hat{\boldsymbol{u}}|$ local minima found for each association of tracks in the orbit-to-orbit real scenario.

$\hat{t}_{M1}$	$\hat{t}_{M2}$	ϵ	$\lvert\hat{\boldsymbol{u}}_1\rvert$ (m/s)	$\lvert\hat{\boldsymbol{u}}_2\rvert$ (m/s)	$\lvert\hat{\boldsymbol{u}}\rvert$ (m/s)
04/12-06:30	04/14-18:30	$3.36 \cdot 10^{-10}$	0.039	1.124	1.163
04/13-06:30	04/13-18:45	$1.65 \cdot 10^{-12}$	0.765	0.404	1.169
04/12-18:30	04/15-06:30	$1.72 \cdot 10^{-10}$	0.251	0.917	1.169
04/12-06:30	04/14-18:45	$1.26 \cdot 10^{-10}$	0.711	0.459	1.170

4. CONCLUSIONS

A novel method for impulsive maneuver detection and estimation for the associations of tracks and orbits during cataloging activities has been presented. The first method focuses on track-to-orbit associations and is intended to estimate single burn maneuvers, by determining the maneuver that applied to the pre-maneuver orbit minimizes the post-maneuver observations residuals. On the contrary, the second method, conceived to solve the orbit-to-orbit association problem, approximates maneuvers of two burns as linear perturbations over the nominal ballistic motion of the RSOs.

These methods can be included in a cataloging chain to increase the flexibility and robustness of the maintenance of the catalog of RSOs. Moreover, they can be integrated in MHT-like frameworks for the evaluation of hypotheses involving tracks and orbits with maneuvers. The detection and estimation of the maneuvers is performed in an optimal control fashion, allowing to retain local minima for the solutions corresponding to different control efforts. In the case of a MHT framework, multiple local minima may translate into the expansion of the association tree, i.e.: generation of new hypotheses related to the maneuver, whereas in a hard-decision framework, this can be reduced to the optimal maneuver, i.e.: that of minimum $|\hat{\boldsymbol{u}}|$. In order to trim the association tree, or avoid taking a wrong decision, a maximum control effort can be defined such that $|\hat{\boldsymbol{u}}| < u_{max}$. The value of u_{max} determines the number of hypotheses that may arise from a maneuver event and also avoid considering unrealistic maneuvers.

It is important to note that these methods have been conceived for the association problem, and therefore, their ultimate goal is not to provide the most accurate or realistic solution, but one that allows the linkage between tracks and orbits (track-to-orbit) and orbits among themselves (orbit-to-orbit). Satellite operators may not always perform optimal maneuvers due to experience, safety or even social aspects and therefore optimal control metrics should not be blindly trusted. At the end, during cataloging operations the final goal is to ensure traceability between tracks and orbits and maximize SST network sensing data usage.

Results for both the track-to-orbit and orbit-to-orbit methods have been obtained for simulated and real observations. The former method shows a good estimation performance for single burn maneuvers, leading to multiple solutions that approach the actual maneuver as the number of post-maneuver tracks increases. Remarkable is the fact that among these solutions, the one with the lowest associated residuals is in fact the most accurate one although the difference in residuals with respect to adjacent solutions is not relevant in some cases.

Finally, the authors would like to mention that the work presented along this paper is part of an on-going PhD research project. The next step, once the performance of the proposed methods have been ensured and studied, is to integrate them into the cataloging chain as explained in Section 1.

Copyright © 2020 Advanced Maui Optical and Space Surveillance Technologies Conference (AMOS) – www.amostech.com

ACKNOWLEDGEMENTS

This project has received funding from the "Comunidad de Madrid" under "Ayudas destinadas a la realización de doctorados industriales" program (project IND2017/TIC7700).

Besides, the authors would like to acknowledge Manuel Sanjurjo-Rivo for his support as student advisor.

REFERENCES

[1] E. Johnston, List of satellites in geostationary orbit (2018).

[2] C. Lafleur, Claude lafleur's spacecraft encyclopedia (2018).

[3] N. L. Johnson, E. Stansbery, D. O. Whitlock, K. J. Abercromby, D. Shoots, History of on-orbit satellite fragmentations, Tech. rep., NASA Orbital Debris Program Office (2008).

[4] J. Stauch, T. Bessell, M. Rutten, J. Baldwin, M. Jah, K. Hill, Joint probabilistic data association and smoothing applied to multiple space object tracking, Journal of Guidance, Control, and Dynamics 41 (1) (2018) 19–33. doi:10.2514/1.G002230.

[5] Y. Bar-Shalom, F. Daum, J. Huang, The probabilistic data association filter, Control Systems, IEEE 29 (2010) 82 – 100. doi:10.1109/MCS.2009.934469.

[6] A. Milani, G. F. Gronchi, M. De' Michieli Vitturi, Z. Knezevic, Orbit determination with very short arcs. i - admissible regions, Celestial Mechanics and Dynamical Astronomy 90 (2004) 57–85. doi:10.1007/s10569-004-6593-5.

[7] L. Pirovano, D. Santeramo, R. Armellin, P. Di Lizia, A. Wittig, Probabilistic data association: the orbit set, Celestial Mechanics and Dynamical Astronomy 132 (02 2020). doi:10.1007/s10569-020-9951-z.

[8] J. Siminski, O. Montenbruck, H. Fiedler, T. Schildknecht, Short-arc tracklet association for geostationary objects, Advances in Space Research 53 (04 2014). doi:10.1016/j.asr.2014.01.017.

[9] R. Furfaro, R. Linares, D. Gaylor, M. Jah, R. Walls, Resident Space Object Characterization and Behavior Understanding via Machine Learning and Ontology-based Bayesian Networks, in: Advanced Maui Optical and Space Surveillance Technologies Conference, 2016, p. 35.

[10] M. Holzinger, D. Scheeres, Object correlation and maneuver detection using optimal control performance metrics, in: Advanced Maui Optical and Space Surveillance Technologies (AMOS) Conference, 2010, p. E26.

[11] M. J. Holzinger, D. J. Scheeres, K. T. Alfriend, Object correlation, maneuver detection, and characterization using control distance metrics, Journal of Guidance, Control, and Dynamics 35 (4) (2012) 1312–1325. doi:10.2514/1.53245.

[12] P. C. Mahalanobis, On the generalised distance in statistics, in: Proceedings of the National Institute of Sciences of India, Vol. 2, 1936, pp. 49–55.

[13] B. Jia, E. Blasch, K. Pham, D. Shen, Z. Wang, X. Tian, G. Chen, Space object tracking and maneuver detection via interacting multiple model cubature kalman filters, IEEE Aerospace Conference Proceedings 2015 (06 2015). doi:10.1109/AERO.2015.7119076.

[14] J. Huang, W. Hu, L. Zhang, Maneuver detection of space object for space surveillance, ESASP 723 (2013) 137.

[15] J. Siminski, T. Schildknecht, T. Flohrer, Assessment of post-maneuver observation correlation using short-arc tracklets, in: Proc. 7th European Conference on Space Debris, Darmstadt, Germany, 18–21 April 2017, (:null), 2017. doi:10.7892/boris.106945.

[16] S. Lemmens, H. Krag, Two-line-elements-based maneuver detection methods for satellites in low earth orbit, Journal of Guidance, Control, and Dynamics 37 (3) (2014) 860–868. doi:10.2514/1.61300.

[17] C. Shabarekh, J. Kent-Bryant, G. Keselman, A. Mitidis, A Novel Method for Satellite Maneuver Prediction, in: Advanced Maui Optical and Space Surveillance Technologies Conference, 2016, p. 11.

[18] A. Pastor, D. Escobar, M. Sanjurjo-Rivo, A. Águeda, Object detection methods for optical survey measurements, in: 20th Advanced Maui Optical and Space Surveillance Technologies, 2019.

[19] K. Hill, C. Sabol, K. T. Alfriend, Comparison of covariance based track association approaches using simulated radar data, The Journal of the Astronautical Sciences 59 (1-2) (2012) 281–300. doi:10.1007/s40295-013-0018-1.

Copyright © 2020 Advanced Maui Optical and Space Surveillance Technologies Conference (AMOS) – www.amostech.com

[20] M. Chernick, S. D'Amico, New closed-form solutions for optimal impulsive control of spacecraft relative motion, Journal of Guidance, Control, and Dynamics 41 (2) (2018) 301–319. doi:10.2514/1.g002848.
[21] N. Ravago, B. A. Jones, Space object maneuver detection in a multi-target environment using a labeled multi-bernoulli filter, in: 1st IAA conference on Space Situational Awareness (ICSSA), 2017, orlando, FL, Nov. 13-15.
[22] J. Siminski, H. Fiedler, T. Flohrer, Correlation of Observations and Orbit Recovery Considering Maneuvers, in: AAS/AIAA Space Flight Mechanics, 2017.
[23] G. M. Goff, Orbit estimation of non-cooperative maneuvering spacecraft, Ph.D. thesis, Department of the Air Force, Air University (2015).
[24] D. Lubey, Maneuver Detection and Reconstruction in Data Sparse Systems with an Optimal Control Based Estimator, Ph.D. thesis, University of Colorado Boulder (Jan. 2015).
[25] O. Montenbruck, E. Gill, Satellite Orbits: Models, Methods and Applications, Springer-Verlag Berlin Heidelberg, 2000. doi:10.1007/978-3-642-58351-3.

Copyright © 2020 Advanced Maui Optical and Space Surveillance Technologies Conference (AMOS) – www.amostech.com